Perpendicular magnetic anisotropy and high spin-polarization ratio in epitaxial Fe-N thin films

Nian Ji,[1,2] M. S. Osofsky,[3] Valeria Lauter,[4] Lawrence F. Allard,[5] Xuan Li,[1] Kevin L. Jensen,[3] Hailemariam Ambaye,[4] Edgar Lara-Curzio,[5] and Jian-Ping Wang[1,2,*]

[1]*The Center for Micromagnetics and Information Technologies and Department of Electrical and Computer Engineering, University of Minnesota, Minneapolis, Minnesota 55455, USA*

[2]*Department of Physics, University of Minnesota, Minneapolis, Minnesota 55455, USA*

[3]*Naval Research Laboratory, 4555 Overlook Avenue SW, Washington, DC 20375, USA*

[4]*Spallation Neutron Source, Oak Ridge National Laboratory, Oak Ridge, Tennessee 37831, USA*

[5]*Materials Science and Technology Division, Oak Ridge National Laboratory, Oak Ridge, Tennessee 37831, USA*

We have demonstrated a general framework for realizing and modulating perpendicular magnetic anisotropy in a rare-earth-element and heavy-metal-free material system. Using GaAs(001)/Fe(001) template, we have developed a synthesis scheme to produce epitaxial body center tetragonal Fe-N with (001) texture. By varying the N doping concentration, the crystal tetragonality (c/a) can be tuned in a relatively wide range. It is found that the Fe-N layer developed a strong perpendicular magnetic crystalline anisotropy (MCA) as it approaches the iron nitride interstitial solubility limit. Further annealing significantly improves the MCA due to the formation of chemically ordered $Fe_{16}N_2$. In addition to realizing an MCA up to 10^7 erg/cm^3, the spin polarization ratio ($P \sim 0.52$), as probed directly by a point-contact Andreev reflection (PCAR) method, even shows a moderate increase in comparison with normal metal Fe ($P \sim 0.45$). These combined properties make this material system a promising candidate for applications in spintronic devices and also potential rare-earth-element free magnets.

I. INTRODUCTION

Giant magnetoresistive devices with perpendicular magnetic anisotropy have drawn increased attention due to their potential for higher storage densities in magnetic memory applications.[1–3] To fabricate such devices, one essential component, the ferromagnetic electrode, which serves as a polarized electron source, has to satisfy two criteria: (1) high value of spin polarization and (2) magnetic easy axis points out of the film plane. The focus of most efforts has been on transition metal (TM) and heavy-elements-based multilayers, which are proven structures with high perpendicular magnetic anisotropy (PMA). However, concerns, such as large damping due to the heavy elements and poor compatibility with the common barrier material, prevent them from being realized in practical applications. For magnetic tunnel junction (MTJ) devices, the recently developed ultra-thin FeCoB layer with PMA offers a new route to tackle the problem, in which a high tunneling magnetoresistance (TMR) (>100%) and an easy axis perpendicular to the film plane are simultaneously realized.[4] However, the utilization of interface anisotropy that produces out-of-plane easy axis demands precise and critical control of layer thicknesses (<1.3 nm) and interface conditions.

Iron nitrides are known to form various phases. Much attention was focused on their saturation magnetization (M_s) due to the debatable claim of giant M_s ($4\pi M_s \sim 3.0$ T) observed on the $Fe_{16}N_2$ phase decades ago.[5–7] Recently, we reported the discovery of the origin of the giant saturation magnetization of such an enigmatic material.[8,9] However, the magnetic anisotropy of this material system has received less attention since most of the known iron nitride phases only possess low magnetocrystalline anisotropy (MCA). In principle, $Fe_{16}N_2$ and its relevant Fe-N martensite form a tetragonal distorted Fe lattice. As a consequence, due to the reduced crystal symmetry, a large MCA is expected to develop, given the reduced energy separation between the two orbitals $d_{x^2-y^2}$ and d_{xy}, which

are located below and above the Fermi level, respectively.[10] Since its a lattice constant (in-plane lattice constant) closely matches that of bcc Fe, this allows the epitaxial control and consequently the realization of an MCA perpendicular to the thin film plane if Fe (001) substrate is provided.

Following this idea, we grew epitaxial Fe-N martensite thin films. We systematically controlled the stoichiometry of Fe-N films using a facing-target sputtering method, which is secondary electron free from substrate with the confined plasma just between the targets.[11–13] Structural characterization based on x-ray diffraction (XRD) and transmission electron microscopy (TEM) imaging reveals the crystal quality and film morphology, which shows that the c axis of the Fe-N layer is perpendicular to the film plane and is coherently adapted on the Fe(001)/GaAs(001) template. A complementary study of magnetometry and polarized neutron reflectometry shows that an MCA perpendicular to the film plane is developed in the Fe-N layer. Moreover, a subsequent postannealing process facilitates the formation of chemically ordered $Fe_{16}N_2$ phase and further enhances the MCA, which is evaluated to exceed 10^7 erg/cm^3. The combination of the large magnetocrystalline anisotropy and its giant saturation magnetization may point a new direction for the synthesis of rare-earth-element free magnets in the future. In addition, we measured the spin polarization ratio of partially ordered $Fe_{16}N_2$ thin films using a point-contact Andreev reflection (PCAR) method,[14] which shows a relatively large spin polarization ratio ($P \sim 0.52$). These combining properties make the $Fe_{16}N_2$ and Fe-N martensites a promising candidate for the ferromagnetic electrodes for future spintronic devices.

II. EXPERIMENTAL AND DISCUSSION

A. Tunable tetragonality of Fe-N martensites

It is known that the α'-Fe-N martensites form interstitial solids and can accommodate N concentration up to $\sim$13 at.%.[15]
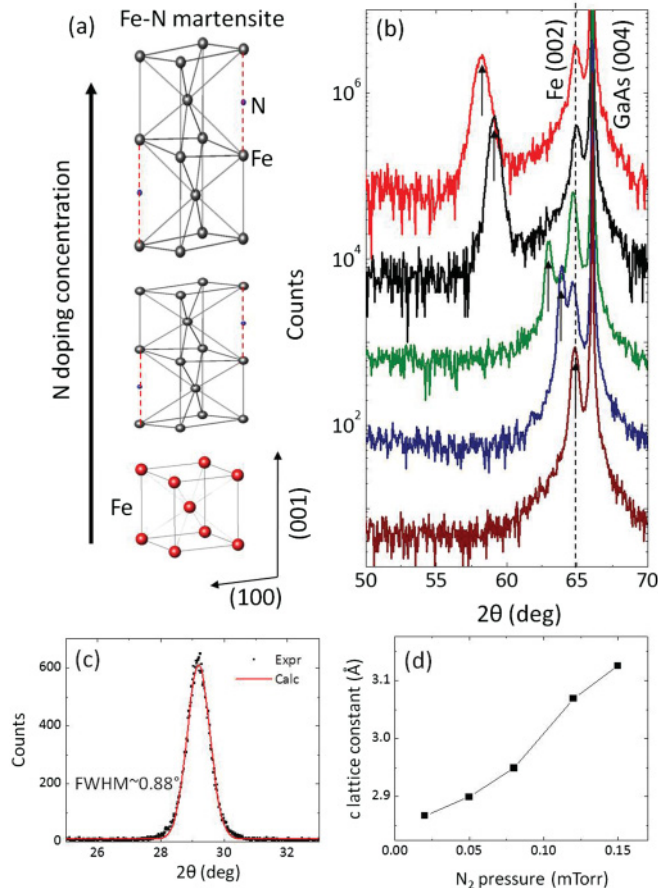
FIG. 1. (Color online) (a) A sketch of different stages of Fe-N tetragonality (c/a) due to the N interstitial doping. (b) X-ray diffraction of as-deposited Fe-N martensite thin films with different c lattice constant. Data from different samples are consistently vertically shifted by a factor of 10 in log scale. The Fe-N (002) peaks shift gradually towards left corresponds to the increase of the N_2 partial pressure during sample growth. (c) Rocking curve measured on Fe-N (002) peak of the sample with largest c lattice constant. (d) Here, c lattice constant calculated from XRD in (b) as a function of N_2 partial pressure in the growth of each sample (all other deposition conditions are kept the same).

In our previous study (Ref. 11), we demonstrated that with an Fe buffer layer providing (001) epitaxial constraint and allowing the increase of the N_2 partial pressure during Fe-N growth, it is possible to epitaxially support the Fe-N martensites with (001) texture. As schematically shown in Fig. 1(a), in principle, by controlling the dopant concentration (N at.%), the c lattice constant can be adjusted while the a lattice is constrained by the underneath Fe buffer layer. As a result, the tetragonality can be fine tuned. In light of these discussions, we systematically fabricated samples with Fe-N layer thicknesses in the range of 45–50 nm using a facing-target sputtering method. Prior to the growth of the Fe-N layer, an Fe layer with a fixed thickness of 22 nm is deposited on a GaAs (001) substrate at temperature of 250 °C to encourage (001) epitaxy at an Ar pressure of 5 mTorr. The subsequent Fe-N layer is prepared by sputtering Fe targets with thoroughly mixed Ar and N_2 working gases (∼1% N_2).
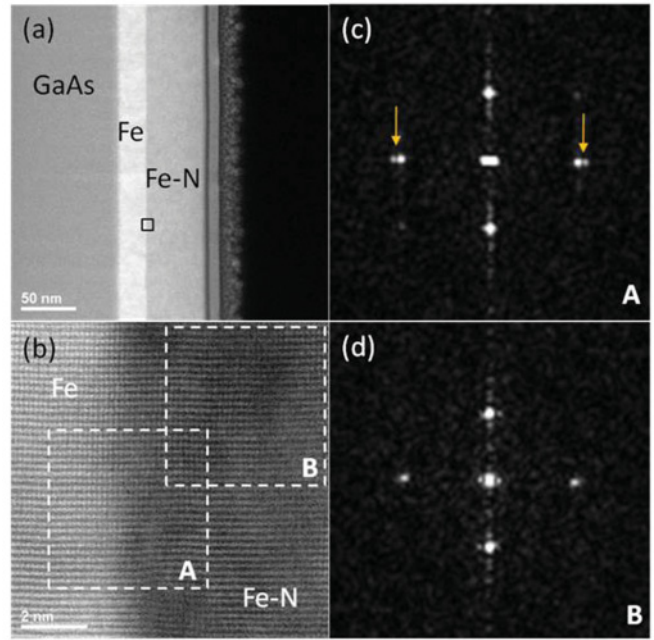

FIG. 2. (Color online) (a) Low-mag HAADF image of a cross-section epitaixial Fe-N martensite thin film. The layered structure at the top interface is due to the Cr and C capping as described in the text. (b) A zoom-in look of the lattice image acquired at the Fe/Fe-N interface [outlined as a box in (a)] with a [110] zone axis. The images within the boxes labeled as A and B are processed by diffractogram, as shown correspondingly in (c) and (d). A clear double peak is shown in A (highlighted by yellow/light gray arrows) corresponding to the lattice periodicity from Fe and Fe-N, respectively. Only one type of lattice periodicity is shown in (d), corresponding to only one d spacing in Fe-N layer.

In Fig. 1(b), the XRD peaks (measured by Philips X"Pert Pro X-ray Diffractometer with Cu Kα radiation) from Fe-N (002) showed a consistent shift towards the lower 2θ values, indicating an elongated d spacing along the (001) direction with a typical texture deviation of $0.88°$ [Fig. 1(c)] according to the rocking curve measured on the Fe-N (002) diffraction peak. This suggests the c lattice constant substantially enhances ($>10\%$) as the N interstitial solubility increases, given the progressively higher N_2 partial pressure [Fig. 1(d)] used in depositing these samples.

To further examine the crystal quality and epitaxial relationship of the present films, we used high-resolution (HR) transmission electron microscopy (TEM) (JEOL 2200FS) to study a cross-sectional sample that may possess the largest c lattice constant according to the XRD. Figure 2(a) shows a high-angle annular dark-field TEM image with low magnification. In addition to the GaAs substrate, Fe and Fe-N layers, as outlined in the figure, Cr cap layer (∼8 nm), and carbon (∼1 μm) layer are deposited *ex situ* for protection from further oxidation. The brightness contrast between two layers is clearly seen, which is due to the presence of the light element N in the Fe-N layer. Aberration-corrected lattice images with nominal resolution of <0.1 nm were recorded at the Fe/Fe-N interface [Fig. 2(b)] to reveal the epitaxy of both layers. To analyze the periodicities, a diffractogram from

a 128 × 128 pixels region (i.e. region A) was computed, and the X and Y scan directions calibrated so that the diffraction spots positions closely matched the known d spacings for the α-Fe structure, as shown in Fig. 2(c). The calculated d spacing matches with a [110] zone axis (axis that is parallel to the observation direction) for both Fe and Fe-N. In addition, the in-plane direction only presents one periodicity, suggesting perfect lattice matching along that direction. Two periodicities are seen in the interface region (box A), indicating the presence of two types of d spacing along film normal. Similar periodicity analysis in the region of Fe-N layer (box B) shows an expected single d spacing and is coherent with the longer-distanced d spacing obtained in analyzing box A. These observations demonstrate the effect of doping N atoms in the crystalline Fe causes a directional expansion of the crystal lattice along c axis perpendicular to the film plane while the in-plane lattice constant (a) is maintained and coherent with the Fe underlayer. The calculated d spacing reasonably matches with that observed by XRD.

B. Magnetic characterization of Fe-N martensites

To systematically study the magnetic properties of these films, first we investigated the in-plane M-H hysteresis loops [Fig. 3(a)] measured by a Princeton Measurements Vibrating Sample Magnetometer at room temperature, which clearly reveal a correlation between the saturation magnetic field [H_s, defined in Fig. 3(b)] and the average c lattice constant as determined from XRD. The selective M-H loops (normalized to saturation magnetization) of these samples are shown in Fig. 3(b). An evolution from typical easy-axis to hard-axis loop is expectedly seen as the c lattice constant of the Fe-N layer progressively increases, with its highest H_s larger than 4 kOe, suggesting an MCA developed in the film due to the presence of Fe-N layer. However, the small but notable M_r suggests the film possesses both in-plane and out-of-plane magnetization components due to the existence of soft Fe underlayer and its strong exchange coupling with the Fe-N layer.

To facilitate the discussion of the magnetic contribution of Fe underlayer, we studied the thickness dependence of in-plane
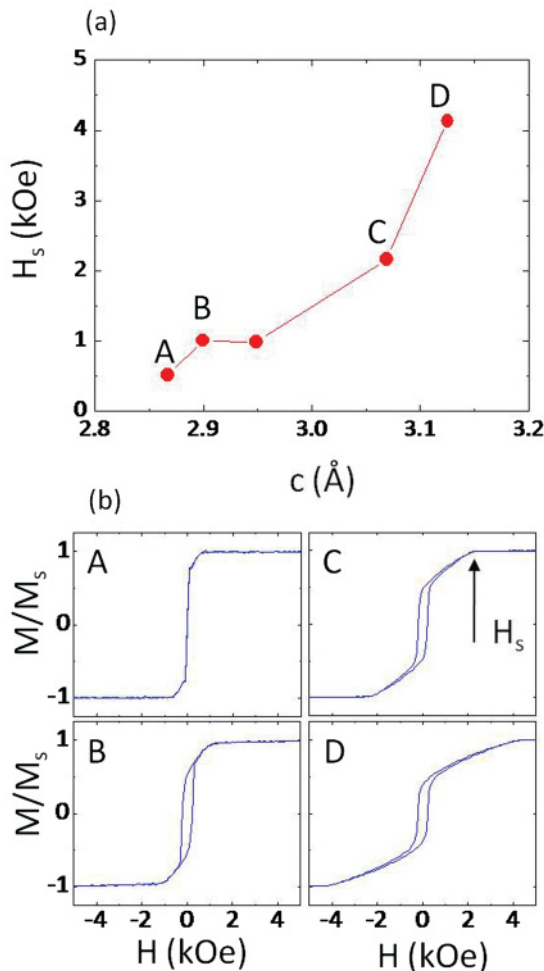

FIG. 3. (Color online) (a) In-plane saturation field (H_s) as a function of the c lattice constant according to XRD results in Fig. 1. (b) Selective M-H loops measured in plane for samples labeled A–D in accordance with that presented in (a). The magnetic field of the point as marked by the arrow in C is the saturation field (H_s) defined in this paper.
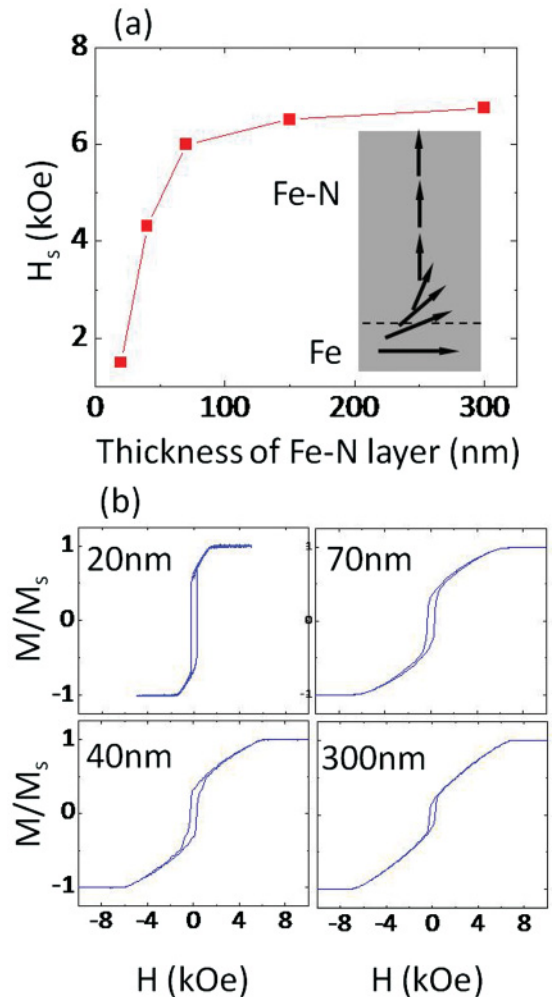

FIG. 4. (Color online) (a) In-plane saturation field (H_s) as a function of thickness of Fe-N layer with same tetragonality (c/a). Inset shows the schematic drawing of magnetization configuration at remanence as explained in the text. (b) Selective M-H loops measured in plane for samples with different Fe-N layer thickness, as outlined in each figure.

M-H loops for samples prepared at N_2 partial pressure of 0.12 mTorr, (deposition condition to fabricate Fe-N films with largest *c/a* ratio). As shown in Figs. 4(a) and 4(b), by increasing the thickness of the Fe-N layer, the saturation field saturates rapidly and levels off at around $H_s \sim 7$ kOe, suggesting the films possesses a remanent (external field $H = 0$) magnetic configuration, as shown in the inset. In particular, as the thickness of the Fe-N layer increases, the magnetic contributions from the underlayer (Fe) and interfacial (Fe/Fe-N) regions become progressively weak. In that case, the saturation field is determined by the crystalline anisotropy of the hard layer towards the top interface. The presence of the typical hard axis loop measured in plane show a clear reversible magnetization rotation process, which provides the evidence of out-of-plane oriented magnetization domains in the Fe-N layer.

C. MCA in partially ordered $Fe_{16}N_2$

Furthermore, in a previous investigation, we showed that a dramatic increase of saturation magnetization (M_s) was observed after *in-situ* postannealing the as-deposited Fe-N

films,[16] which is attributed to the presence of chemically ordered $Fe_{16}N_2$ and is associated with the increase of N site ordering (D). Here, by systematically analyzing *M-H* loops of optimally annealed (120 °C for 40 h) samples with the same bilayer structure, we show that the H_s also increases monotonically.

In Fig. 5(a), the XRD patterns of an as-deposited and an annealed sample with the same nominal structure [Fe-N(48 nm)/Fe(22 nm/GaAs)] were compared. The main difference occurs at $2\theta = 28.6°$, where the XRD pattern of the annealed sample develops a robust peak and can be indexed to $Fe_{16}N_2(002)$, originated from the superlattice diffraction given the alternating occupancy of N in crystalline $Fe_{16}N_2$ [inset of Fig. 5(a)]. By analyzing the integrated intensity ratio between (002) and (004) peaks, it is possible to estimate the volume fraction of the $Fe_{16}N_2$ in the Fe-N layer. To facilitate the discussion, we introduced a parameter D, which describes the degree of N ordering as shown in detail previously (Ref. 16) The in-plane *M-H* loops of both samples are compared in Fig. 5(b). It is seen that H_s increased substantially in the annealed sample. More samples with
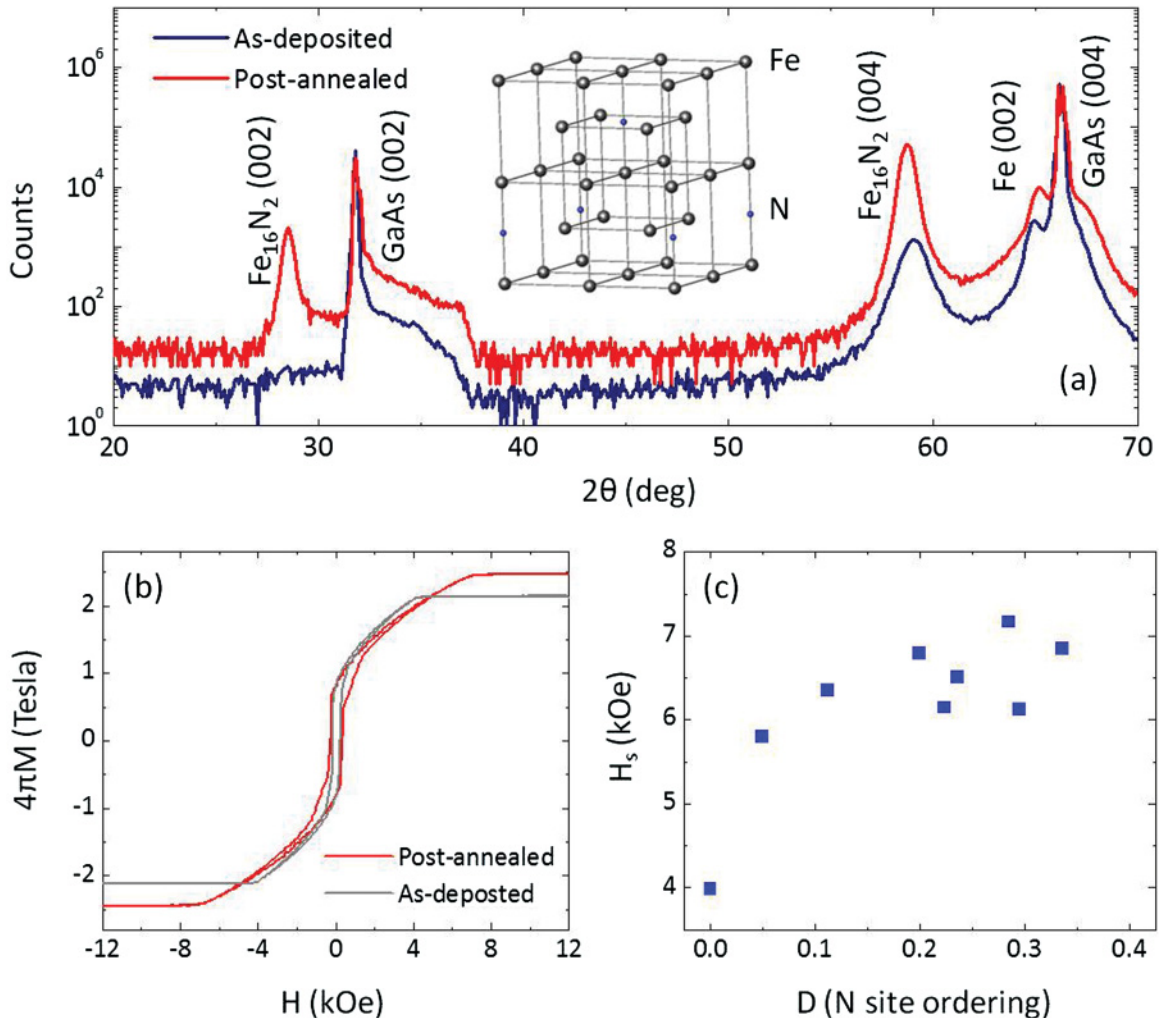

FIG. 5. (Color online) (a) X-ray diffraction pattern of as-deposited and annealed samples with similar structure [Fe-N(48 nm)/Fe(22 nm)GaAs]. The inset shows the crystal unit cell of $Fe_{16}N_2$. The ordered site occupation of the N atoms causes the diffraction of $Fe_{16}N_2(002)$, which is not seen in the as-deposited sample. (b) *M-H* loops measured in plane for the two samples shown in (a). (c) In-plane saturation field (H_s) as a function of N site ordering D as defined in Ref. 12.
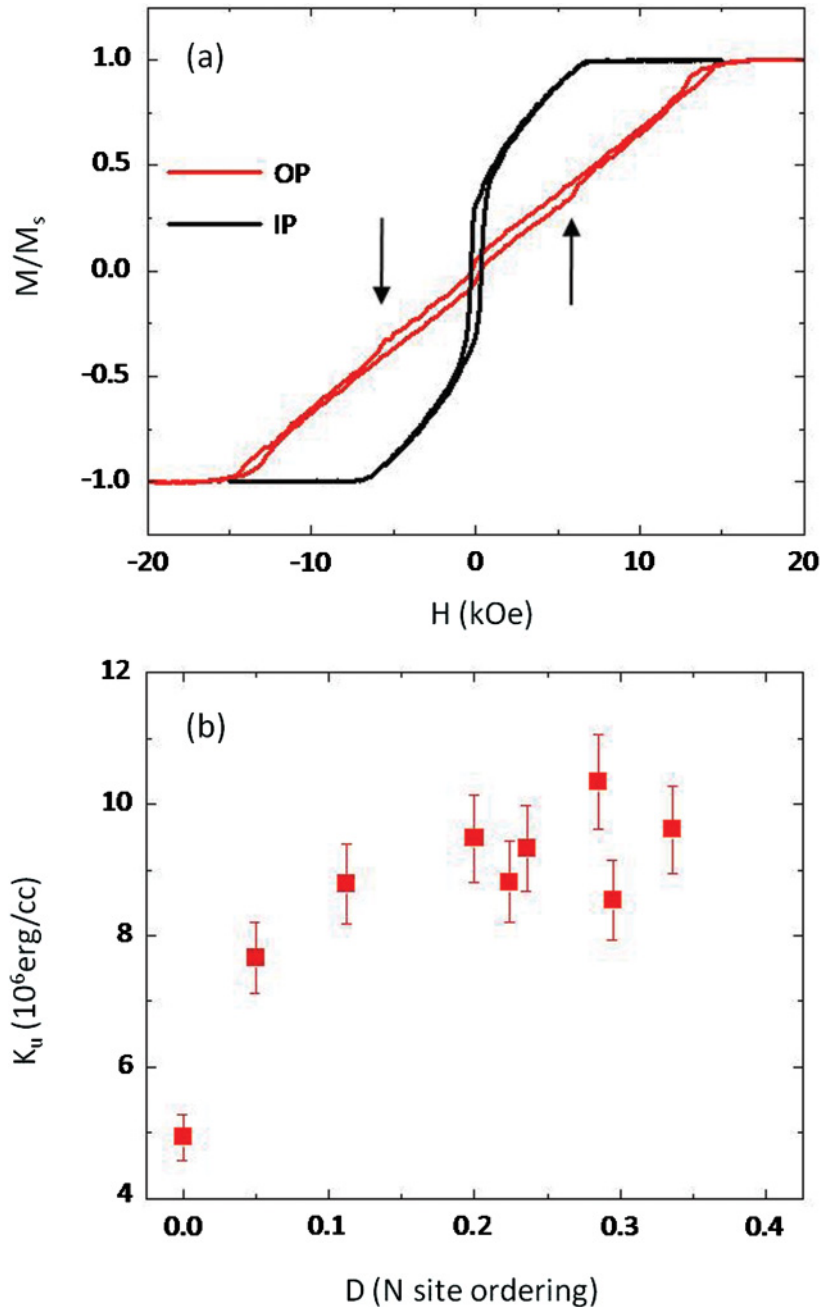
FIG. 6. (Color online) (a) In-plane (solid) and out-of-plane (dash) M-H loops measured on one partially ordered $Fe_{16}N_2$ sample ($D \sim 0.32$). The Fe-N layer switches at $H_c \sim 5.7$ kOe (black arrows). (b) Calculated K_u as a function of degree of N site ordering (D) in partially ordered $Fe_{16}N_2$ thin film samples as described in text. The dashed line here is a guide to the eye. All the samples have the same nominal thickness structure: Fe-N(48 nm)/Fe (22 nm)/GaAs.

different D values are compared in Fig. 5(c), in which a correlation between D and H_s is clearly seen.

To further evaluate the magnetic configuration in more details, both in-plane and out-of-plane M-H loops for a partially ordered sample ($D = 0.32$) are shown in Fig. 6(a). As for the out-of-plane loop, as stated above, due to the magnetic contribution of the Fe layer, the samples develop both in-plane and out-of-plane magnetization components at remanence state, as schematically shown in the inset of Fig. 4(a). As a result, the in-plane magnetization component causes the large demagnetization linear background up to about 16 kOe in order to fully saturate the sample along the out-of-plane direction. However, at an applied field of $H \sim 5.7$ kOe, a switching is clearly seen which is originated from the magnetization

flip of the out-of-plane component in the Fe-N layer. For a rough estimation, the H_s measured in plane coincides with the larger switching point measured out of plane, suggesting the anisotropy field H_k is close to H_s with crystalline anisotropy (K_u) aligning perpendicular to film plane. Therefore, we can calculate[17] the crystalline anisotropy in the Fe-N layer as a function of N site ordering after knowing the saturation magnetization (M_s) of Fe-N layer [Fig. 6(b)]. The highest K_u is seen around $\sim 10^7$ erg/cc, which agrees well with the previous reported value determined by torque curve measurements (Ref. 7). It is worth mentioning that the present synthesis process (deposition and postannealing) does not produce phase-pure $Fe_{16}N_2$ from the structural analysis. In particular, the highest volume fraction of the $Fe_{16}N_2$ in the Fe-N layer, which
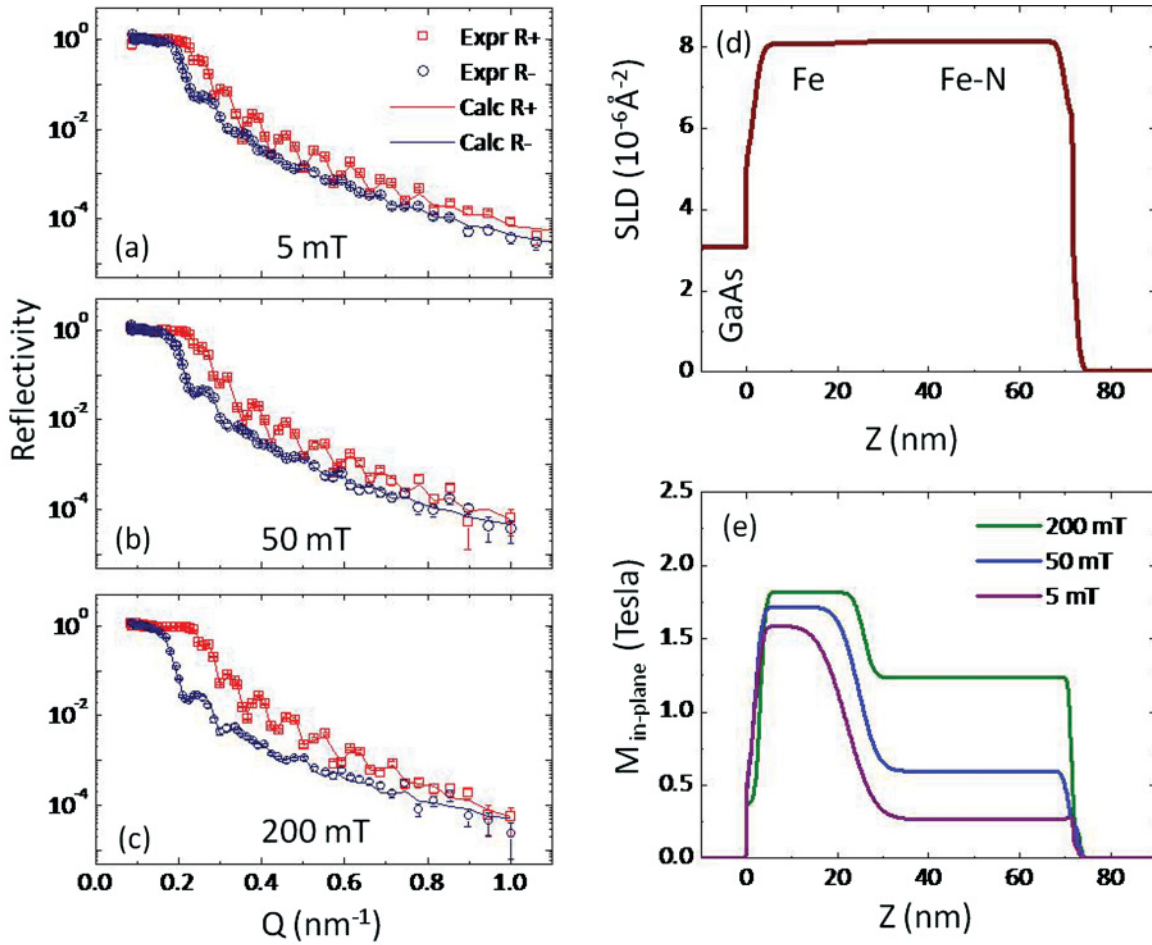
FIG. 7. (Color online) (a)–(c) Fitted polarized neutron with spin-up (R^+) and spin-down (R^-) reflectivity curves for an annealed sample at external field of 5, 50, and 200 mT. (d) Nuclear scattering length density and (e) field dependent in-plane magnetization depth profiles as functions from the distance from the substrate.

consists of $Fe_{16}N_2$ and Fe_8N, has been obtained to be ~39% according to the XRD analysis using the current sputtering fabrication process. However, the increasing trend of the K_u upon the degree of N ordering increases clearly shows that the MCA should be much higher for pure-phase $Fe_{16}N_2$.

D. Polarized neutron reflectometry

To confirm the magnetic configuration based on the hysteresis loop analysis, in-depth and field-dependence polarized neutron reflectometry (PNR) experiments were performed using the Magnetism Reflectometer on Beamline 4A at Spallation Neutron Source, Oak Ridge National Laboratory.[18] This is a time-of-flight (TOF) instrument with a wavelength band of 2–5 Å and a polarization efficiency of ~98%. When conducting the PNR experiments, an external magnetic field was applied parallel to the thin film plane. The nonspin-flip reflectivity curves of spin-up and spin-down neutrons were spontaneously recorded. Representative fitted PNR spectra for one partially ordered sample are shown in Figs. 7(a)–7(c), in which three different in-plane fields smaller than the H_s are purposely

chosen after saturating the sample at around $H_s = 20$ kOe. With the nuclear scattering length density (NSLD) closely matching the nominal value [Fig. 7(d)], the spontaneously fitted in-plane projection of the magnetization depth profile [$M(z)_{\text{in-plane}}$] was retrieved [Fig. 7(e)]. It is seen that, in contrast to that of the Fe layer, the in-plane component of the magnetization vector $M(z)_{\text{in-plane}}$ of the Fe-N layer goes down drastically with decreasing in-plane external field. This can have two scenarios. In the first one, the Fe-N film forms nearly antiferromagnetic in-plane domains. In the second one, the film magnetization turns out of plane due to the out-of-plane easy axis. The first scenario is possible only if the Fe-N film would have uniaxial in-plane anisotropy, which is not the case. In addition in the first scenario, a strong magnetic off-specular scattering would appear. However, we did not record an increase in the off-specular scattering. In the second scenario, no additional off-specular scattering is expected, because the out-of-plane component of the magnetization vector is parallel to the momentum transfer Q, and the in-plane parallel component contributes to the specular reflection. Hence, the reduction of the in-plane magnetization originates from the evolution of the out-of-plane magnetization component along
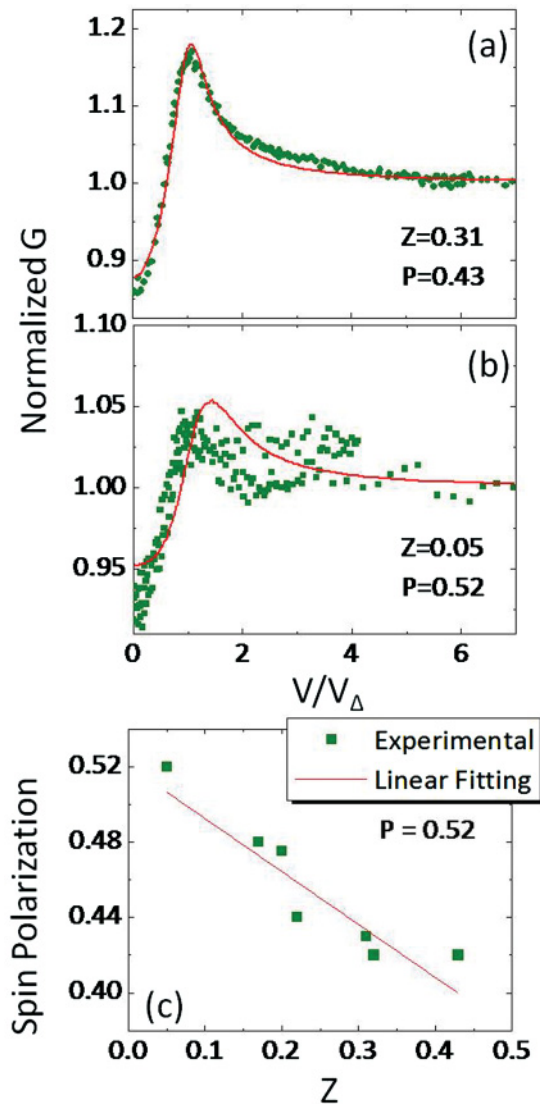
FIG. 8. (Color online) Point-contact Andreev reflection measurement on partially ordered $Fe_{16}N_2$ with structure Fe-N(48 nm)/Fe(22 nm)/GaAs. (a) and (b) Normalized conductance as a function of applied voltage (V) divided by superconducting gap (V_Δ). Experimental data is shown in dots (green/gray) and fitting is shown in continues curve (red/dark gray). (c) Spin polarization as a function of Z (described in text), the experiment data (green/gray dots) is fitted linearly (straight line).

E. Spin-polarization ratio measurement

Encouraged by the magnetic characterization, we performed a direct measurement of the transport spin polarization (SP) using PCAR (Ref. 14) on a partially ordered $Fe_{16}N_2$ sample in Fig. 8. A superconducting (Nb) tip was gently pressed into the sample to minimize the effect of surface oxidation. At least 10 such different contacts were created and tested at a temperature of 1.6 K. Figures 8(a) and 8(b) show normalized conductance $G(V)/G_n$ vs V/V_Δ, in which G_n is the conductance at applied voltage $V \gg V_\Delta$ and V_Δ is the superconducting gap of Nb. The PCAR experimental curves were fitted by the modified[19] Blonder-Tinkham-Klapwijk (BTK) model[20] with the fitting parameters spin polarization P and barrier strength Z. The superconducting gap Δ was fixed to the value for Nb. An effective temperature (3.5 K) was used to improve the quality of the fit for low Z junctions [Fig. 8(b)], suggesting that electron heating was occurring. The noise observed in the data is relatively large, which is attributed to the weak signal produced as the SP is close to 0.5. Fits based on a ballistic model reproduces the experimental data reasonably well, producing an apparent dependence of P on Z. As a result, the intrinsic spin-polarization value was obtained by extrapolating the result to $Z = 0$.[21] Figure 4(c) shows the linear fit of P vs Z, which intercepts $Z = 0$ at 0.52, namely the spin polarization of our sample approximates 52%. In comparison with reported values of ∼45% on Fe samples using similar probing approaches,[22] the present results show moderate enhancement.

III. SUMMARY

In conclusion, we have spontaneously realized perpendicular mangetocrystalline anisotropy (MCA) and high spin-polarization ratio (SP) by a simple scheme, namely, tuning the c lattice constant of bcc Fe by interstitial doping of N. The in-plane lattice parameter of the present Fe-N films is close to bcc Fe, allowing a direct epitaxial adaption with an MgO barrier for MTJ and a Ag spacer for giant magnetoresistance (GMR) applications. Furthermore, utilizing light-element (e.g. B, C, and N) and ferromagnetic (e.g. Fe, Co, and Ni) interstitial alloys to develop magnetic material with strong perpendicular MCA without using any rare earth elements offers a promising approach for developing new magnet materials for clean energy applications.

the perpendicular easy axes. It is worth mentioning that the oscillation magnitude of the R^- curve is relatively small comparing to R^+. Since the oscillation magnitude is directly related to the SLD contrast between the film and the substrate. This observation is likely due to the SLD of the R^- being very close to that of the substrate in contrast to the SLD of R^+. This effect is especially robust as it approaches the bottom interface (GaAs/Fe), in which case the scattering behavior of that region is dominated by the reflectivity at high q_z and consequently results in the smearing out of the oscillation magnitude.

*jpwang@umn.edu

[1] H. Meng and J. P. Wang, Appl. Phys. Lett. **88**, 172506 (2006).

[2] S. Mangin, D. Ravelosona1, J. A. Katine, M. J. Carey, B. D. Terris, and Eric E. Fullerton, Nat. Mater. **5**, 210 (2006).

[3] T. Seki, S. Mitani, K. Yakushiji, and K. Takanashi, Appl. Phys. Lett. **88**, 172504 (2006).

[4] S. Ikeda, K. Miura, H. Yamamoto, K. Mizunuma, H. D. Gan, M. Endo, S. Kanai, J. Hayakawa, F. Matsukura, and H. Ohno, Nat. Mater. **9**, 721 (2010).

[5] T. K. Kim and M. Takahashi, Appl. Phys. Lett. **20**, 492 (1972); Y. Sugita, K. Mitsuoka, M. Komuro, H. Hoshiya, Y. Kozono, and M. Hanazono, J. Appl. Phys. **70**, 5977 (1991); M. Takahashi, H. Shoji, H. Takahashi, H. Nashi, T. Wakiyama, M. Doi, and M. Matsui, *ibid.* **76**, 6642 (1994).

[6] At the Annual Conference on Magnetism and Magnetic Materials in 1996, a symposium was held on the topic Fe16N2, on which both theorists and experimentalists presented their work. The papers were published in J. Appl. Phys. **79**, 5564 (1996). No decisive conclusion was drawn on whether it has giant saturation magnetization. This has been mainly due to the lack of a convincing theory and unavailability of repeatable samples. This topic has been largely dropped by the research community of magnetic materials and magnetism since then.

[7] H. Takahashi, M. Igarashi, A. Kaneko, H. Miyajima, and Y. Sugita, IEEE Trans. Magn. **35**, 2982 (1999).

[8] N. Ji, X. Liu, and J. P. Wang, New J. Phys. **12**, 063032 (2010).

[9] X. Liu, Y.-H. Xu, C. Sanchez-Hanke, and J.-P. Wang, e-print arXiv:0909.4478 (2009); J. P. Wang, N. Ji, X. Q. Liu, Y. Xu, C. Sánchez-Hanke, Y. Wu, F. M. F. de Groot, L. F. Allard, and E. Lara-Curzio, IEEE Trans. Magn. (in press, 2012).

[10] P. Bruno, Phys. Rev. B **39**, 865 (1989).

[11] N. Ji, Y. Wu, and J.-P. Wang, J. Appl. Phys. **109**, 07B767 (2011).

[12] J. R. Shi and J. P. Wang, Thin Solid Films **420**, 172 (2002).

[13] Z. H. Qian, G. Wang, J. M. Sivertsen, and J. H. Judy, IEEE Trans. Magn. **33**, 3748 (1997).

[14] R. J. Soulen Jr., J. M. Byers, M. S. Osofsky, B. Nadgorny, T. Ambrose, S. F. Cheng, P. R. Broussard, C. T. Tanaka, J. Nowak, J. S. Moodera, A. Barry, and J. M. D. Coey, Science **282**, 85 (1998).

[15] K. H. Jack, Proc. R. Soc. London Ser. A **208**, 200 (1951).

[16] N. Ji, L. F. Allard, E. Lara-Curzio, and J. P. Wang, Appl. Phys. Lett. **98**, 092506 (2011).

[17] To calculate the K_u, we used the equation: $K_u = H_k \times M_s/2$, where M_s is the saturation magnetization of the Fe-N layer and H_k is H_s as defined in text.

[18] V. Lauter, H. Ambaye, R. Goyette, W. T. H. Lee, and A. Parizzi, Physica B **404**, 2543 (2009); V. Lauter-Pasyuk, J. Phys. IV France 1 (2007); V. Lauter-Pasyuk, H. J. Lauter, B. P. Toperverg, L. Romashev, and V. Ustinov, Phys. Rev. Lett. **89**, 167203 (2002).

[19] I. I. Mazin, A. A. Golubov, and B. Nadgorny, J. Appl. Phys. **89**, 7576 (2001); G. T. Woods, R. J. Soulen Jr., I. I. Mazin, B. Nadgorny, M. S. Osofsky, J. Sanders, H. Srikanth, W. F. Egelhoff, and R. Datla, Phys. Rev. B **70**, 054416 (2004).

[20] G. E. Blonder, M. Tinkham, and T. M. Klapwijk, Phys. Rev. B **25**, 4515 (1982).

[21] Y. Ji, C. L. Chien, Y. Tomioka, and Y. Tokura, Phys. Rev. B **66**, 012410 (2002); Y. Ji, G. J. Strijkers, F. Y. Yang, C. L. Chien, J. M. Byers, A. Anguelouch, G. Xiao, and A. Gupta, Phys. Rev. Lett. **86**, 5585 (2001); P. Raychaudhuri, A. P. Mackenzie, J. W. Reiner, and M. R. Beasley, Phys. Rev. B **67**, 020411 (2003); C. H. Kant, O. Kurnosikov, A. T. Filip, P. LeClair, H. J. M. Swagten, and W. J. M. de Jonge, *ibid.* **66**, 212403 (2002).

[22] B. Nadgorny, R. J. Soulen Jr., M. S. Osofsky, I. I. Mazin, G. Laprade, R. J. M. van de Veerdonk, A. A. Smits, S. F. Cheng, E. F. Skelton, and S. B. Qadri, Phys. Rev. B **61**, R3788 (2000).